

# Prompt-Enhanced Self-supervised Representation Learning for Remote Sensing Image Understanding

Mingming Zhang, Qingjie Liu, and Yunhong Wang

State Key Laboratory of Virtual Reality Technology and Systems, Beihang University  
Beijing, China

## Abstract

Learning representations through self-supervision on a large-scale, unlabeled dataset has proven to be highly effective for understanding diverse images, such as those used in remote sensing image analysis. However, remote sensing images often have complex and densely populated scenes, with multiple land objects and no clear foreground objects. This intrinsic property can lead to false positive pairs in contrastive learning, or missing contextual information in reconstructive learning, which can limit the effectiveness of existing self-supervised learning methods. To address these problems, we propose a prompt-enhanced self-supervised representation learning method that uses a simple yet efficient pre-training pipeline. Our approach involves utilizing original image patches as a reconstructive prompt template, and designing a prompt-enhanced generative branch that provides contextual information through semantic consistency constraints. We collected a dataset of over 1.28 million remote sensing images that is comparable to the popular ImageNet dataset, but without specific temporal or geographical constraints. Our experiments show that our method outperforms fully supervised learning models and state-of-the-art self-supervised learning methods on various downstream tasks, including land cover classification, semantic segmentation, object detection, and instance segmentation. These results demonstrate that our approach learns impressive remote sensing representations with high generalization and transferability.

## 1. Introduction

Remote sensing images have been widely used in many applications, including precision agriculture, disaster management, city planning, and environment monitoring. With a growing number of satellites collecting remote sensing images ceaselessly, abundant remote sensing images are easy to access, but annotations are technically challenging due to highly time-consuming and expertise knowledge

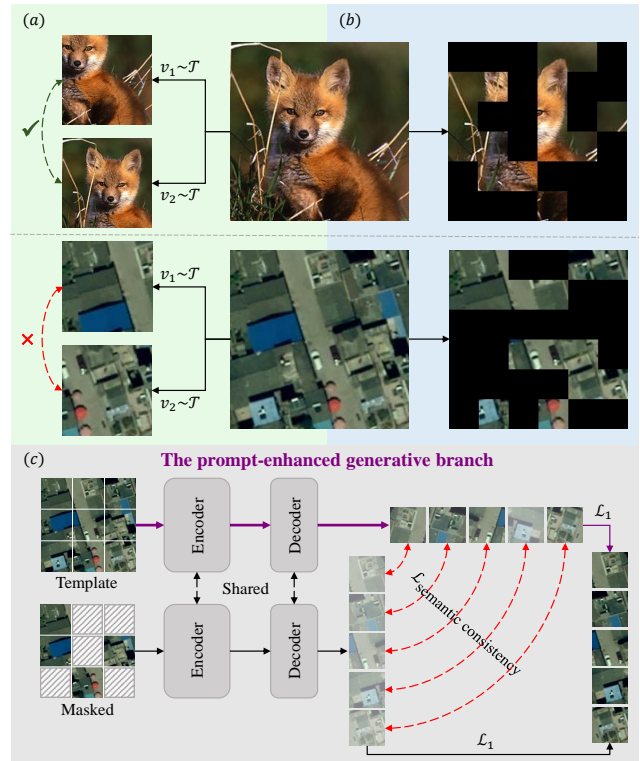


Figure 1. Object density differs between natural and remote sensing images. Remote sensing images contain multiple objects, especially no apparent foreground objects, resulting in challenges for SSL: (a) false positive pairs or (b) missing contextual information. (c) Our pre-training pipeline introduces a prompt-enhanced generative branch to provide contextual information by the semantic consistency constraint.

than general benchmark datasets, *e.g.*, ImageNet [42]. Recently, self-supervised learning (SSL) has been increasingly emerging to pre-train models on large unlabeled data and demonstrate stronger performance than supervised learning on classification, segmentation, and detection. Therefore, the SSL paradigm has been receiving much attention from the community and explored to obtain an efficient pre-

trained model on large-scale data for remote sensing image understanding.

Existing SSL methods in computer vision can be classified into contrastive and reconstructive learning methods. Contrastive learning methods minimize the distance between representations of two views augmented from one image (*i.e.*, positive pairs), while reconstructive learning methods learn representations by solving the reconstructive pre-text task from masked images. Although many attempts based on contrastive or reconstructive learning have improved performance for remote sensing image analysis, these remote sensing SSL methods still have some limitations due to the considerably high object density in remote sensing images. Natural images typically have apparent foreground objects in a relatively simple background, *e.g.*, the fox in Figure 1. However, remote sensing images contain multiple objects in a vast complicated scene and typically have no apparent foreground objects since they are captured by sensors mounted on satellites, as illustrated in Figure 1. Therefore, SSL for remote sensing analysis remains significant challenges as follows:

(1) *False positive pairs.* Figure 1(a) shows false positive pairs augmented from one remote sensing image. This makes contrastive learning much less effective since positive pairs play a crucial role in representation learning. Existing contrastive learning methods [3, 38] leverage the spatial-temporal structure to organize positive pairs for representation learning. However, learned representations should be sensitive to image pairs that have large changes in the temporal span, such as major urban development [37] and disasters. Due to the limitations of the pre-training data structure, these methods introduce additional complex designs on data organization or pretext tasks, resulting in a complex pre-training pipeline and limited performance when transferring to remote sensing tasks.

(2) *Missing contextual information.* General masked images, like the fox in Figure 1(b), can be easily repaired by inferring the whole from some parts through rich contextual information. However, some small land objects may be entirely masked out by the randomly masking operation compared with natural images, as shown in Figure 1(b). Due to missing contextual information, this would hamper semantic extrapolating for remote sensing representation learning during the reconstruction. SatMAE [11] masks remote sensing images carefully across multi-spectral and temporal dimensions to pre-train the network, which still does not solve the missing contextual information problem and limits its generalization ability.

We rethink: *is SSL paradigm really effective for remote sensing representation learning?* We explore this answer from the characteristics of remote sensing data and tasks. Since most remote sensing tasks are dense predictions at object-level or pixel-level that require high-resolution fea-

tures with fine-grained details, contrastive learning obtains image-level features by comparing two images, thus leading to less optimal in remote sensing analysis. Although reconstructive learning learns features with fine-grained information, it suffers from semantic reasoning by missing contextual information due to the greatly high object density of remote sensing data. We argue that the original patches masked in the reconstruction can be formulated as reconstructive prompt templates. Based on the templates, a prompt-enhanced module is embedded in the SSL pipeline to make the reconstruction mimicking feature extraction and learning semantic extrapolating by providing meaningful contextual information. Additionally, existing SSL methods take great care to construct pre-training datasets by leveraging the spatial-temporal structure, resulting in poor generalization and transferring ability, further preventing research on the larger scale model and dataset collection. Since SSL methods require large-scale unlabeled data, the natural advantage of abundant remote sensing images captured by sensors daily should be reconsidered.

Motivated by the observation, we propose a novel **Prompt-enhanced self-supervised representation learning** method based on **ReConstructive learning (PReCo)** to learn representations with high-level semantic and fine-grained details for remote sensing image analysis. PReCo first adopts a pixel reconstructive pre-text task to capture local information from the masked image. Then, a prompt-enhanced generative branch formulates the original patches as the reconstructive prompt template, which is introduced to provide contextual information by the semantic consistency constraint. To train PReCo, a large-scale unlabeled dataset is collected, which contains over 1.28 million images that is comparable to the generic pre-training ImageNet [42]. Moreover, we collect the pre-training dataset without carefully designed in terms of temporal and geographical dimensions, making the model and dataset easily extended to a larger scale in further research.

We evaluate our approach on different tasks, including single-label and multi-label land cover classification, semantic segmentation, object detection, and instance segmentation. Following other remote sensing SSL methods, we use BigEarthNet [45], EuroSAT [22], xView [27], and SpaceNet [50] for comparison. Extensive experiments demonstrate that our method outperforms existing remote sensing SSL methods (up to +2.95%) and is more effective for remote sensing tasks than supervised learning on the common ImageNet [42] (up to +5.24%). In summary, our contributions are:

1. We propose a novel prompt-enhanced self-supervised representation learning method based on reconstructive learning (called PReCo), a simple pre-training pipeline to learn robust and transferable representations for efficient remote sensing image analysis.

2. PReCo formulates the original image patches as the reconstructive prompt template and introduces a prompt-enhanced generative branch based on the analysis that remote sensing images have greatly high object density than natural images, which typically contain dense and small land cover objects in a vast and complex scene. The prompt-enhanced generative branch provides contextual information by the semantic consistency constraint during the reconstruction.
3. By pre-training on a large-scale unlabeled dataset, PReCo learns representations with rich semantic and local information, which benefits image-level, object-level, and pixel-level downstream tasks in remote sensing applications. Moreover, we achieve state-of-the-art performance on single-label and multi-label land cover classification, semantic segmentation, object detection, and instance segmentation, comprehensively demonstrating its transferability and superiority for remote sensing image analysis.

## 2. Related Work

### 2.1. Contrastive Learning

Contrastive learning methods [7–9, 15, 32, 40, 48, 57] can learn good representations by minimizing the distance between representations of two views augmented from one image (*i.e.*, positive pairs) and pushing the negative pairs from different images away. Recent contrastive learning methods [16, 26, 41, 58] have demonstrated their superiority in transferring to downstream tasks, even outperforming supervised learning. Although increasingly successful in many computer vision tasks, contrastive learning methods consider more image-level features, limiting the transferring performance in dense prediction cases requiring more local details.

### 2.2. Reconstructive Learning

Inspired by BERT [12] for masked language modeling, recent reconstructive learning methods [5, 20, 36, 54, 55] learn representations through solving the reconstructive pretext task after employing a special [MASK] token to mask a portion of image patches randomly. MAE [20] first handles visible patches in the encoder, then encoded patches and mask tokens are processed in the decoder, which can significantly reduce the computation overhead of the encoder. SimMIM [55] only uses a lightweight prediction head to reconstruct raw pixel values of masked patches, facilitating good representation learning of the encoder. MixMAE [34] reconstructs two original images from the mixed image by replacing the original masked patches with visible patches of another image, improving pre-training efficiency and maintaining pretraining-finetuning consistency. With SOTA performance on many computer vision tasks, many

related works have been studied, such as VideoMAE [49], MultiMAE [4], CIM [14], MSN [2], and SiamMAE [17]. However, these works have yet to be explored on large-scale remote sensing datasets.

### 2.3. Self-Supervised Learning in Remote Sensing

Recently, self-supervised learning has been broadly applied in remote sensing domains. For instance, [24, 25, 29, 44, 51] utilize contrastive learning to learn representations. SeCo [38] contrastively learns seasonal invariance by constructing a remote sensing dataset of different temporal information. [3, 30, 31] consider that geographical knowledge is the unique characteristic of remote sensing images, which can be used for contrastive learning. Inspired by classical material and texture methods, MATTER [1] leverages multi-temporal, spatially aligned remote sensing imagery over unchanged regions to learn representations invariance to illumination and viewing angle, finally achieving consistency of material and texture representations. Another attempt explores the masked image modeling paradigm for remote sensing feature pre-training by repairing masked images, such as [46, 52]. SatMAE [11] based on Masked Autoencoder (MAE) leverages temporal and multi-spectral information for pre-training the network. Besides, more relevant works have been studied for special tasks, including change detection [6, 10, 53], land cover classification [23, 43, 56], and semantic segmentation [21, 28, 39, 47].

While many methods show improved performance on different downstream tasks, these methods are pre-trained on datasets by carefully organizing in terms of temporal and geographical dimensions, leading to poor generalization ability. Besides, the gap in object density information between natural and remote sensing images needs to be reconsidered. Since remote sensing images contain multiple interesting objects rather than one obvious foreground object in natural images, existing remote sensing SSL methods remain challenging in the acquisition of positive pairs and reconstruction of masked image patches. This work designs self-supervised representation learning based on reconstruction with a prompt-enhanced generative branch, which can learn representations with rich semantic and fine-grained details.

## 3. Method

Figure 2 shows the pre-training pipeline of PReCo, and we will describe the main components in the following.

### 3.1. Overview

Our proposed PReCo is a novel prompt-enhanced self-supervised representation learning method based on reconstructive learning. Following the vision transformer, *e.g.*, ViT [13], PReCo first uniformly splits an input  $x$  into non-overlapping image patches  $x^p$  and then randomly mask  $x^p$

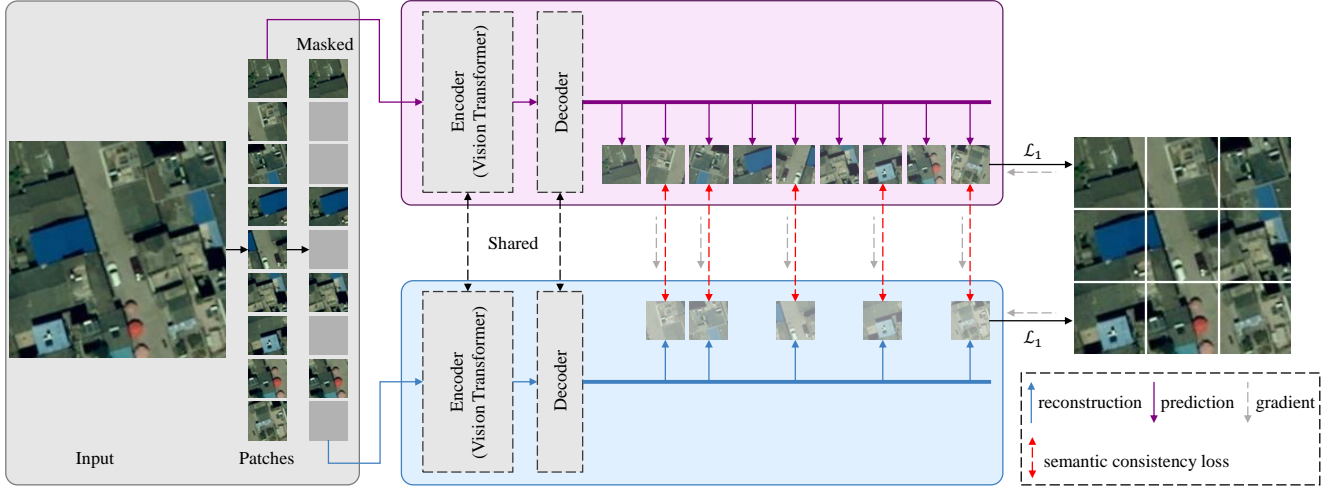


Figure 2. An illustration of PReCo, a simple yet efficient pre-training framework for remote sensing tasks. PReCo introduces a novel prompt-enhanced generative branch to provide contextual information by the semantic consistency constraint during the reconstruction, which formulates the original image patches as the reconstructive prompt template. PReCo learns highly generalizable and transferable representations for various downstream tasks (e.g., image-level, object-level, and pixel-level).

on patch-level to obtain a new input patches  $\hat{x}^p$ . Subsequently, PReCo takes as input  $\hat{x}^p$  to reconstruct the raw pixel values of the masked patches through the encoder-decoder architecture. Unlike natural images, the object density of remote sensing images is extremely uneven, resulting in false positive pairs or missing contextual information in SSL. To tackle this issue, we represent the original image patches as reconstructive prompt templates rather than directly removing the masked patches, and introduce a prompt-enhanced generative branch to facilitate semantic reasoning by providing meaningful contextual information during the reconstruction. Moreover, the prompt-enhanced generative branch shares the encoder and the decoder with the reconstructive branch. Finally, our proposed PReCo is pre-trained on a large-scale unlabeled dataset and learns impressive representations, which is beneficial for various downstream tasks (e.g., image-level, object-level, and pixel-level).

### 3.2. Reconstruction of masked image patches

In the reconstruction stage, PReCo aims to learn local fine-grained features by restoring masked image patches. Given an input image  $x \in \mathbb{R}^{C \times H \times W}$ , PReCo firstly reshapes  $x$  to get image sequence patches  $x^p \in \mathbb{R}^{N \times P^2 C}$ , where  $H, W, C$  are the image height, width, and channel, respectively,  $P$  is the size of each image patch (i.e., the height and width), and  $N = (H/P) \cdot (W/P)$  is the number of image patches. Then, a patch-wise masking operation randomly masks some image patches, and a patch embedding operation encodes each image patch to get the new sequence input  $\hat{x}^p$ . Subsequently, an encoder  $f_\theta$  takes the sequence

input  $\hat{x}^p$  to extract latent representations  $\hat{h}^p$ , which are used in downstream tasks after pre-training. Finally, a decoder  $g_\theta$  is used to reconstruct pixel values of masked patches  $\hat{y}^p$  on the latent representations. In our paper, we take Swin Transformer [35] as the feature encoder  $f_{swin}$  and a lightweight prediction head as the decoder  $g_{mlp}$  to output raw pixel values of the masked patches by following SimMIM [55], which can be formulated as:

$$\hat{y}^p = g_{mlp}(f_{swin}(\hat{x}^p) \odot \mathbb{I}_{\mathcal{M}}(\hat{x}_i^p)) \quad (1)$$

where  $\mathbb{I}_{\mathcal{M}}(\cdot)$  is an indicator function that is 1 when each image patch  $\hat{x}_i^p$  is masked, 0 otherwise.  $\odot$  is an element-wise product operation.

### 3.3. Prompt-enhanced generative branch

Compared with natural images that captured in daily scenes and objects are mostly with large size, remote sensing images typically cover multiple land objects with a large-scale and complex scene, which have no clear foreground objects. Therefore, some small land covers could be entirely masked, resulting in missing critical contextual information during the reconstruction. To tackle this issue, PReCo introduces a prompt-enhanced generative branch to provide contextual information. As illustrated in Figure 2, the prompt-enhanced generative branch inputs the image patches  $x^p$  to extract latent representations  $h^p$  with rich contextual information by the shared encoder  $f_\theta$ . Then, the latent representations  $h^p$  are fed to the same decoder  $g_\theta$  to predict the raw pixels  $y^p$ . In addition, contrastive learning is also integrated into the proposed PReCo from the perspective that  $x^p$  and  $\hat{x}^p$  can be recast as two augmented views from one image,

prompting the encoder to learn more discriminative features with high-level semantic information.

### 3.4. Training objective

PReCo first realizes a reconstructive learning objective by minimizing the distance between raw pixel values  $X$  and the reconstructive values  $Y_{Re}$ :

$$L_{Re} = \frac{\|Y_{Re} - X\|}{N} \quad (2)$$

where  $N$  is the number of masked pixels.  $\|\cdot\|$  is a distance function for calculating similarity between  $Y_{Re}$  and  $X$  (e.g.,  $L_1$  or  $L_2$  loss).

For the prompt-enhanced generative branch, PReCo adopts the Equation 2 to learn contextual information by calculating the predicted loss  $L_{Pr}$  between the predicted pixel values  $Y_{Pr}$  and raw pixel values  $X$ . Then, a semantic consistency loss  $L_{Sc}$  maximizes the similarity between  $Y_{Re}$  and the corresponding portion of  $Y_{Pr}$ , which is defined as:

$$L_{Sc} = \text{Dist}(Y_{Re} - Y_{Pr}) \quad (3)$$

where  $\text{Dist}(\cdot)$  is a similarity function to guide PReCo learning good contextual information.

Finally, the joint training objective is:

$$L = \lambda_{Re} \cdot L_{Re} + \lambda_{Pr} \cdot L_{Pr} + \lambda_{Sc} \cdot L_{Sc} \quad (4)$$

where  $\lambda_{Re}$ ,  $\lambda_{Pr}$ , and  $\lambda_{Sc}$  are weighting coefficients balancing different modules of PReCo. PReCo learns representations with rich semantic and local information by pre-training in a multi-task learning manner.

## 4. Experiments

This section describes the dataset and the experiment settings. To evaluate learned representations, quantitative and qualitative results on remote sensing tasks are discussed in detail. Furthermore, we conduct ablation studies to verify the effectiveness of the proposed pre-training framework.

### 4.1. Pre-training

**Dataset.** Existing methods carefully construct the pre-training dataset in temporal and geographic dimensions, limiting the generalization and transferring ability of the pre-trained representations. In our work, we collect a large-scale unlabeled remote sensing dataset captured from the WorldView-3 over various regions. Some examples of the dataset are shown in Figure 3. In our experiments, we crop images into  $192 \times 192$  pixels and get 1,287,248 image patches to train PReCo.

**Implementation Details.** We adopt Swin-B as the encoder. All experiments are implemented by the PyTorch framework with 8 NVIDIA Tesla V100 GPUs. We use AdamW



Figure 3. Pre-training dataset in our work, which consists of 1.28M images comparable to ImageNet.

optimizer with hyper-parameters  $\beta_1 = 0.9$ ,  $\beta_2 = 0.999$ , and  $\epsilon = 1 \times 10^{-8}$ , and the learning rate is set to  $1 \times 10^{-5}$ . The training last for 200 epochs with a batch size of 112 per GPU.

### 4.2. Transfer Learning Settings

In downstream experiments, we select single-label land cover classification, multi-label land cover classification, semantic segmentation, object detection, and instance segmentation, covering image-level, object-level, and pixel-level remote sensing tasks. To comprehensively confirm the performance of our method, we compare PReCo with contrastive learning methods (SeCo [38], Ayush, et al. [3], and MATTER [1]) and a SOTA reconstructive learning method SatMAE [1]. Following the comparison methods, we use EuroSAT [22], BigEarthNet [45], SpaceNet (Rio) [50], xView [27], and SpaceNet (Las Vegas) [50] to evaluate different tasks. Furthermore, we also compare with supervised learning from ImageNet pre-training and random initialization, which adopts ResNet-50 [18] and Swin Transformer [35] as two different backbones. Especially, R50\_Random, R50\_IN, and Swin-B\_IN shown in Tabs. 1 to 6 denote that the supervised learning method of different backbones (ResNet-50 and Swin-B) initialized with different weights (random initialization and ImageNet pre-training), respectively. Finally, extensive experiments show that PReCo has strong performance on downstream tasks.

### 4.3. Land Cover Classification on EuroSAT

**Implementation Details.** EuroSAT [22] is a single-label land cover classification dataset composing of Sentinel-2 satellite images. EuroSAT contains ten classes and has 27,000 labeled images with a size of  $64 \times 64$ . Following SeCo [38] and SatMAE [11], we adopt the official train/val splits on the EuroSAT.

For the single-label land cover classification experiment, we initialize a Swin-B backbone with the pre-trained weight and fine-tune a linear classifier head on top with ground truth labels in a supervised manner. We use an AdamW op-

Method	Top-1 Accuracy $\uparrow$
Sup. (R50_Random)	55.32
Sup. (R50_IN)	89.08
Sup. (Swin-B_IN)	95.77
SeCo [38]	95.43
Ayush et al. [3]	96.38
SatMAE [11]	95.74
PReCo (ours)	<b>98.69</b>

Table 1. Top-1 accuracy on the EuroSAT for single-label land cover classification. PReCo gets the best performance.

timizer, a batch size of 32, a learning rate of  $8 \times 10^{-5}$ , and finally report the top-1 accuracy for performance comparison. Since MATTER [1] does not evaluate performance on the EuroSAT, we compare our method with the other comparison methods.

**Quantitative Results.** Table 1 shows the top-1 accuracy of the different methods using fully supervised and self-supervised training. We can see that PReCo outperforms the ImageNet supervised Swin-B backbone by +2.92%, illustrating that SSL on a large-scale remote sensing dataset improves performance for remote sensing downstream tasks. Compared with contrastive and reconstructive learning methods, PReCo respectively achieves +2.31% and +2.95% higher top-1 accuracy, demonstrating that our approach learns robust and good transferable remote sensing representations for different downstream tasks.

#### 4.4. Land Cover Classification on BigEarthNet

**Implementation Details.** BigEarthNet [45] is a large-scale Sentinel-2 dataset comprising 590,326 images across ten Europe countries. Each image is annotated with 19 classes, so we report the mean average precision (mAP) of all categories to measure the performance of different methods. Following SeCo [38] and MATTER [1], we omit patches covered by seasonal snow, clouds, or cloud shadows and use the same train/val splits for this experiment.

We fine-tune a classifier head on top of a pre-trained Swin-B backbone. We use an AdamW optimizer, a batch size of 96, a learning rate of 0.0001, and a weight decay of 0.005. We use 10% of the train set to evaluate the label efficient transfer learning followed by SatMAE [11].

**Quantitative Results.** In Table 2, PReCo is compared with SeCo [38] and MATTER [1] due to no performance evaluation on the whole training set for Ayush et al. [3] and SatMAE [11]. We observe that PReCo improves the model of the Swin-B backbone initialized with the ImageNet supervised pre-training by +3.26% higher, proving that the domain gap exists between natural and remote sensing images. Table 3 reports the performance of different methods on 10% of BigEarthNet’s labeled data, except for MAT-

Method	mAP $\uparrow$
Sup. (R50_Random)	78.98
Sup. (R50_IN)	86.74
Sup. (Swin-B_IN)	83.62
SeCo [38]	87.81
MATTER [1]	<b>87.98</b>
PReCo (ours)	86.88

Table 2. Mean average precision (mAP) on the BigEarthNet for multi-label land cover classification.

Method	mAP $\uparrow$
Sup. (R50_Random)	69.49
Sup. (R50_IN)	80.04
Sup. (Swin-B_IN)	78.77
SeCo [38]	82.62
Ayush et al. [3]	80.20
SatMAE [11]	82.13
PReCo (ours)	<b>82.67</b>

Table 3. Label-efficient transfer learning on 10% of the BigEarthNet. Our method is more label-efficient than other comparison methods.

TER [1] due to no performance evaluation for this setting. We find that PReCo outperforms ImageNet supervised pre-training with the Swin-B backbone by +3.9% and achieves +0.54% higher than SatMAE [11]. Extensive experiments show that PReCo is more label-efficient than other comparison methods.

#### 4.5. Semantic Segmentation

**Implementation Details.** We use SpaceNet (Rio) dataset [50] for the semantic segmentation task. This dataset contains 6,940 satellite images with binary building masks.

Following SatMAE [11], we fine-tune a PSANet [59] with the pre-trained Swin-B backbone by PReCo. We use an AdamW optimizer with a batch size of 8, a learning rate of  $6 \times 10^{-5}$ , and a weight decay of 0.01. We report mean intersection over union (mIoU) to compare PReCo with comparison methods, except for MATTER [1] due to no evaluation for this experiment setting.

**Quantitative Results.** Table 4 presents mIoU values on the SpaceNet (Rio) of different methods. The results show that our method achieves more considerable performance gains by +5.24% for supervised learning from the ImageNet pre-trained weight with the Swin-B backbone and +1.4% compared with SatMAE [11]. Consistent experimental results demonstrate the effectiveness of our method for the semantic segmentation task.

Method	mIoU $\uparrow$
Sup. (R50_Random)	75.57
Sup. (R50_IN)	75.61
Sup. (Swin-B_IN)	74.23
SeCo [38]	77.09
Ayush et al. [3]	78.51
SatMAE [11]	78.07
PReCo (ours)	<b>79.47</b>

Table 4. Mean intersection over union (mIoU) on the SpaceNet (Rio) semantic segmentation task. Our method consistently improves supervised learning and self-supervised learning by large margins.

Method	$AP_{50} \uparrow$
Sup. (R50_Random)	14.42
Sup. (R50_IN)	14.44
Sup. (Swin-B_IN)	16.30
SeCo [38]	8.9
Ayush et al. [3]	17.74
PReCo (ours)	<b>18.80</b>

Table 5.  $AP_{50}$  on the xView object detection task. Our method improves the SOTA method by +1.06%, demonstrating its transferability for object detection.

## 4.6. Object Detection

**Implementation Details.** Following Ayush et al. [3], we use the xView dataset [27] to verify the object detection performance. The xView dataset contains 846 satellite images with a size of about  $3000 \times 2000$  pixels at 0.3m ground sample distance. This dataset has 60 categories with bounding box annotation and is split into  $416 \times 416$  pixels. Then, we fine-tune a RetinaNet [33] with an AdamW optimizer, a batch size of 4, a learning rate of  $1 \times 10^{-5}$ , and a weight decay of 0.05. We use the indicator  $AP_{50}$  to compare PReCo with SeCo [38] and Ayush et al. [3] that evaluate performance on this task.

**Quantitative Results.** Table 5 lists results from comprehensive experiments on the xView dataset compared with supervised and self-supervised learning. PReCo achieves 18.80%  $AP_{50}$ , improving the self-supervised learning method [3] by +1.06%. The extraordinary performance demonstrates that PReCo learns impressive representations for object detection tasks.

## 4.7. Instance Segmentation

**Implementation Details.** The SpaceNet (LasVegas) dataset [50] is used for instance segmentation, consisting of 3851 images across Las Vegas. The size of images is  $650 \times 650$  pixels with a spatial resolution of 30 cm/pixel.

Method	$AP^m$	$AP_{50}^m$	$AP_{75}^m$
Sup. (R50_Random)	58.2	86.2	70.1
Sup. (R50_IN)	60.2	86.9	72.7
Sup. (Swin-B_IN)	59.1	86.8	70.7
SeCo [38]	58.4	86.5	70.5
Ayush et al. *	58.9	86.6	70.8
SatMAE [11]	52.4	83.7	61.1
PReCo (ours)	<b>60.5</b>	<b>87.8</b>	<b>72.9</b>

Table 6.  $AP^m$ ,  $AP_{50}^m$ , and  $AP_{75}^m$  on the SpaceNet (Las Vegas) instance segmentation task. PReCo outperforms comparison methods (+1.4% and +1.6% for supervised and self-supervised learning, respectively). \* denotes the method [3].

Method	LcC (Acc.)	SS (mIoU)	OD ( $AP_{50}$ )	IS ( $AP^m$ )
PReCo (ours)	<b>98.69</b>	<b>79.47</b>	<b>18.80</b>	<b>60.50</b>
- P-E	96.90	76.91	16.30	59.10

Table 7. Ablation study. LcC, SS, OD, and IS denote land cover classification, semantic segmentation, object detection, and instance segmentation, respectively. ‘- P-E’ removes the prompt-enhanced generative branch from PReCo.

In our experiment, this dataset is randomly divided into train/test/validation subsets with a ratio of 8:1:1. We fine-tune MaskRCNN [19] with the pre-trained Swin-B backbone from our PReCo on the SpaceNet (LasVegas), using an AdamW optimizer, a learning rate of 0.0001, a batch size of 8. Finally, we report the  $AP^m$ ,  $AP_{50}^m$ , and  $AP_{75}^m$  under different intersection over union (IoU) thresholds in the segmentation level.

**Quantitative Results.** As shown in Table 6, our approach learns transferable representations outperforming all the comparison methods. Especially, PReCo improves the ImageNet supervised pre-training with the Swin-B backbone by +1.4%  $AP^m$ , +1%  $AP_{50}^m$ , and +2.2%  $AP_{75}^m$ , respectively. Moreover, PReCo achieves +8.1%  $AP^m$ , +4.1%  $AP_{50}^m$ , and +11.8%  $AP_{75}^m$  higher compared with SatMAE [11]. The impressive results illustrate that PReCo learns good representations with high-level semantic and fine-grained details.

## 4.8. Qualitative Results

Figure 4 shows the visualization comparison of Mask RCNN on the SpaceNet (Las Vegas) from different pre-training methods, comprehensively illustrating the transferability of representations. From qualitative results, PReCo generates high-quality instance segmentation of different sizes and shapes, demonstrating that PReCo learns more transferable features for remote sensing image analysis.



Figure 4. Qualitative results of Mask RCNN on the SpaceNet (Las Vegas) initialized with different pre-training weights to show feature transferability. PReCo generates high-quality masks of different sizes and shapes, demonstrating that PReCo learns more transferable features for remote sensing image analysis. Zoom in for a clearer view.

#### 4.9. Ablation Study

We conduct ablation studies to verify the effectiveness of the designed prompt-enhanced generative branch with four typical tasks on the EuroSAT, SpaceNet (Rio), xView, and SpaceNet (Las Vegas), respectively. In Table 7, ablation results have confirmed that the prompt-enhanced generative branch can significantly improve the performance (up to +2.56%), illustrating its effectiveness.

### 5. Conclusion

This paper presents PReCo, a novel prompt-enhanced reconstructive learning pipeline for remote sensing representation learning from a large-scale unlabeled dataset. PReCo formulates the original patches as reconstructive prompt templates and designs a prompt-enhanced generative branch

to provide contextual information using the semantic consistency constraint. To train PReCo, an unlabeled remote sensing dataset is collected without carefully designed, containing over 1.28 million images. Comprehensive experiments on land cover classification, semantic segmentation, object detection, and instance segmentation demonstrate that PReCo learns impressive representations with high generalization and transferable ability, significantly outperforming fully supervised and self-supervised learning methods.

With the simple pipeline and the solid performance, we hope this work will inspire other works, not just in the remote sensing community but also in the industry and medical image analysis community.

## References

- [1] Peri Akiva, Matthew Purri, and Matthew Leotta. Self-supervised material and texture representation learning for remote sensing tasks. In *IEEE Conference on Computer Vision and Pattern Recognition (CVPR)*, pages 8203–8215, 2022. [3](#), [5](#), [6](#)
- [2] Mahmoud Assran, Mathilde Caron, Ishan Misra, Piotr Bojanowski, Florian Bordes, Pascal Vincent, Armand Joulin, Mike Rabbat, and Nicolas Ballas. Masked siamese networks for label-efficient learning. In *European Conference on Computer Vision (ECCV)*, pages 456–473, 2022. [3](#)
- [3] Kumar Ayush, Burak Uzkent, Chenlin Meng, Kumar Tanmay, Marshall Burke, David Lobell, and Stefano Ermon. Geography-aware self-supervised learning. In *IEEE International Conference on Computer Vision (ICCV)*, pages 10181–10190, 2021. [2](#), [3](#), [5](#), [6](#), [7](#)
- [4] Roman Bachmann, David Mizrahi, Andrei Atanov, and Amir Zamir. Multimae: Multi-modal multi-task masked autoencoders. In *European Conference on Computer Vision (ECCV)*, pages 348–367, 2022. [3](#)
- [5] Hangbo Bao, Li Dong, Songhao Piao, and Furu Wei. Beit: Bert pre-training of image transformers. *arXiv preprint arXiv:2106.08254*, 2021. [3](#)
- [6] Hao Chen, Wenyuan Li, Song Chen, and Zhenwei Shi. Semantic-aware dense representation learning for remote sensing image change detection. *IEEE Transactions on Geoscience and Remote Sensing*, 60:1–18, 2022. [3](#)
- [7] Ting Chen, Simon Kornblith, Mohammad Norouzi, and Geoffrey Hinton. A simple framework for contrastive learning of visual representations. In *International Conference on Machine Learning (ICML)*, pages 1597–1607, 2020. [3](#)
- [8] Xinlei Chen and Kaiming He. Exploring simple siamese representation learning. In *IEEE Conference on Computer Vision and Pattern Recognition (CVPR)*, pages 15750–15758, 2021.
- [9] Xinlei Chen, Haoqi Fan, Ross Girshick, and Kaiming He. Improved baselines with momentum contrastive learning. *arXiv preprint arXiv:2003.04297*, 2020. [3](#)
- [10] Yuxing Chen and Lorenzo Bruzzone. Self-supervised change detection in multiview remote sensing images. *IEEE Transactions on Geoscience and Remote Sensing*, 60:1–12, 2022. [3](#)
- [11] Yezhen Cong, Samar Khanna, Chenlin Meng, Patrick Liu, Erik Rozi, Yutong He, Marshall Burke, David Lobell, and Stefano Ermon. Satmae: Pre-training transformers for temporal and multi-spectral satellite imagery. *Advances in Neural Information Processing Systems (NeurIPS)*, 35:197–211, 2022. [2](#), [3](#), [5](#), [6](#), [7](#)
- [12] Jacob Devlin, Ming-Wei Chang, Kenton Lee, and Kristina Toutanova. Bert: Pre-training of deep bidirectional transformers for language understanding. *arXiv preprint arXiv:1810.04805*, 2018. [3](#)
- [13] Alexey Dosovitskiy, Lucas Beyer, Alexander Kolesnikov, Dirk Weissenborn, Xiaohua Zhai, Thomas Unterthiner, Mostafa Dehghani, Matthias Minderer, Georg Heigold, Sylvain Gelly, Jakob Uszkoreit, and Neil Houlsby. An image is worth 16x16 words: Transformers for image recognition at scale. *International Conference on Learning Representations (ICLR)*, 2021. [3](#)
- [14] Yuxin Fang, Li Dong, Hangbo Bao, Xinggang Wang, and Furu Wei. Corrupted image modeling for self-supervised visual pre-training. *arXiv preprint arXiv:2202.03382*, 2022. [3](#)
- [15] Jean-Bastien Grill, Florian Strub, Florent Altché, Corentin Tallec, Pierre Richemond, Elena Buchatskaya, Carl Doersch, Bernardo Avila Pires, Zhaohan Guo, Mohammad Gheshlaghi Azar, et al. Bootstrap your own latent—a new approach to self-supervised learning. *Advances in Neural Information Processing Systems (NeurIPS)*, 33:21271–21284, 2020. [3](#)
- [16] Tianyu Guo, Hong Liu, Zhan Chen, Mengyuan Liu, Tao Wang, and Runwei Ding. Contrastive learning from extremely augmented skeleton sequences for self-supervised action recognition. In *AAAI Conference on Artificial Intelligence*, pages 762–770, 2022. [3](#)
- [17] Agrim Gupta, Jiajun Wu, Jia Deng, and Li Fei-Fei. Siamese masked autoencoders. *arXiv preprint arXiv:2305.14344*, 2023. [3](#)
- [18] Kaiming He, Xiangyu Zhang, Shaoqing Ren, and Jian Sun. Deep residual learning for image recognition. In *IEEE Conference on Computer Vision and Pattern Recognition (CVPR)*, pages 770–778, 2016. [5](#)
- [19] Kaiming He, Georgia Gkioxari, Piotr Dollár, and Ross Girshick. Mask r-cnn. In *IEEE International Conference on Computer Vision (ICCV)*, pages 2961–2969, 2017. [7](#)
- [20] Kaiming He, Xinlei Chen, Saining Xie, Yanghao Li, Piotr Dollár, and Ross Girshick. Masked autoencoders are scalable vision learners. In *IEEE Conference on Computer Vision and Pattern Recognition (CVPR)*, pages 16000–16009, 2022. [3](#)
- [21] Shuyi He, Qingyong Li, Yang Liu, and Wen Wang. Semantic segmentation of remote sensing images with self-supervised semantic-aware inpainting. *IEEE Geoscience and Remote Sensing Letters*, 19:1–5, 2022. [3](#)
- [22] Patrick Helber, Benjamin Bischke, Andreas Dengel, and Damian Borth. Eurosat: A novel dataset and deep learning benchmark for land use and land cover classification. *IEEE Journal of Selected Topics in Applied Earth Observations and Remote Sensing*, 12(7):2217–2226, 2019. [2](#), [5](#)
- [23] Haozhe Huang, Zhongfeng Mou, Yuning Li, Qiujuan Li, Jie Chen, and Haifeng Li. Spatial-temporal invariant contrastive learning for remote sensing scene classification. *IEEE Geoscience and Remote Sensing Letters*, 19:1–5, 2022. [3](#)
- [24] Heechul Jung, Yoonju Oh, Seongho Jeong, Chaehyeon Lee, and Taegyun Jeon. Contrastive self-supervised learning with smoothed representation for remote sensing. *IEEE Geoscience and Remote Sensing Letters*, 19:1–5, 2021. [3](#)
- [25] Jian Kang, Ruben Fernandez-Beltran, Puhong Duan, Sicong Liu, and Antonio J Plaza. Deep unsupervised embedding for remotely sensed images based on spatially augmented momentum contrast. *IEEE Transactions on Geoscience and Remote Sensing*, 59(3):2598–2610, 2020. [3](#)
- [26] Daeha Kim and Byung Cheol Song. Contrastive adversarial learning for person independent facial emotion recognition. In *AAAI Conference on Artificial Intelligence*, pages 5948–5956, 2021. [3](#)

- [27] Darius Lam, Richard Kuzma, Kevin McGee, Samuel Dooley, Michael Laielli, Matthew Klaric, Yaroslav Bulatov, and Brendan McCord. xviv: Objects in context in overhead imagery. *arXiv preprint arXiv:1802.07856*, 2018. 2, 5, 7
- [28] Haifeng Li, Yi Li, Guo Zhang, Ruoyun Liu, Haozhe Huang, Qing Zhu, and Chao Tao. Global and local contrastive self-supervised learning for semantic segmentation of hr remote sensing images. *IEEE Transactions on Geoscience and Remote Sensing*, 60:1–14, 2022. 3
- [29] Wenyuan Li, Hao Chen, and Zhenwei Shi. Semantic segmentation of remote sensing images with self-supervised multi-task representation learning. *IEEE Journal of Selected Topics in Applied Earth Observations and Remote Sensing*, 14:6438–6450, 2021. 3
- [30] Wenyuan Li, Keyan Chen, Hao Chen, and Zhenwei Shi. Geographical knowledge-driven representation learning for remote sensing images. *IEEE Transactions on Geoscience and Remote Sensing*, 60:1–16, 2021. 3
- [31] Wenyuan Li, Keyan Chen, and Zhenwei Shi. Geographical supervision correction for remote sensing representation learning. *IEEE Transactions on Geoscience and Remote Sensing*, 60:1–20, 2022. 3
- [32] Yunfan Li, Peng Hu, Zitao Liu, Dezhong Peng, Joey Tianyi Zhou, and Xi Peng. Contrastive clustering. In *AAAI conference on Artificial Intelligence*, pages 8547–8555, 2021. 3
- [33] Tsung-Yi Lin, Priya Goyal, Ross Girshick, Kaiming He, and Piotr Dollár. Focal loss for dense object detection. In *IEEE International Conference on Computer Vision (ICCV)*, pages 2980–2988, 2017. 7
- [34] Jihao Liu, Xin Huang, Jinliang Zheng, Yu Liu, and Hongsheng Li. Mixmae: Mixed and masked autoencoder for efficient pretraining of hierarchical vision transformers. In *IEEE Conference on Computer Vision and Pattern Recognition (CVPR)*, pages 6252–6261, 2023. 3
- [35] Ze Liu, Yutong Lin, Yue Cao, Han Hu, Yixuan Wei, Zheng Zhang, Stephen Lin, and Baining Guo. Swin transformer: Hierarchical vision transformer using shifted windows. In *IEEE International Conference on Computer Vision (ICCV)*, pages 10012–10022, 2021. 4, 5
- [36] Zhengqi Liu, Jie Gui, and Hao Luo. Good helper is around you: Attention-driven masked image modeling. In *AAAI Conference on Artificial Intelligence*, pages 1799–1807, 2023. 3
- [37] Utkarsh Mall, Bharath Hariharan, and Kavita Bala. Change-aware sampling and contrastive learning for satellite images. In *IEEE Conference on Computer Vision and Pattern Recognition (CVPR)*, pages 5261–5270, 2023. 2
- [38] Oscar Manas, Alexandre Lacoste, Xavier Giró-i Nieto, David Vazquez, and Pau Rodriguez. Seasonal contrast: Unsupervised pre-training from uncurated remote sensing data. In *IEEE International Conference on Computer Vision (ICCV)*, pages 9414–9423, 2021. 2, 3, 5, 6, 7
- [39] Dilxat Muhtar, Xueliang Zhang, and Pengfeng Xiao. Index your position: A novel self-supervised learning method for remote sensing images semantic segmentation. *IEEE Transactions on Geoscience and Remote Sensing*, 60:1–11, 2022. 3
- [40] Aaron van den Oord, Yazhe Li, and Oriol Vinyals. Representation learning with contrastive predictive coding. *arXiv preprint arXiv:1807.03748*, 2018. 3
- [41] Tal Reiss and Yedid Hoshen. Mean-shifted contrastive loss for anomaly detection. In *AAAI Conference on Artificial Intelligence*, pages 2155–2162, 2023. 3
- [42] Olga Russakovsky, Jia Deng, Hao Su, Jonathan Krause, Sanjeev Satheesh, Sean Ma, Zhiheng Huang, Andrej Karpathy, Aditya Khosla, Michael Bernstein, et al. Imagenet large scale visual recognition challenge. *International Journal of Computer Vision (IJCV)*, 115:211–252, 2015. 1, 2
- [43] Linus Scheibenreif, Joëlle Hanna, Michael Mommert, and Damian Borth. Self-supervised vision transformers for land-cover segmentation and classification. In *IEEE Conference on Computer Vision and Pattern Recognition (CVPR)*, pages 1422–1431, 2022. 3
- [44] Vladan Stojnic and Vladimir Risojevic. Self-supervised learning of remote sensing scene representations using contrastive multiview coding. In *IEEE Conference on Computer Vision and Pattern Recognition (CVPR)*, pages 1182–1191, 2021. 3
- [45] Gencer Sumbul, Marcela Charfuelan, Begüm Demir, and Volker Markl. Bigearthnet: A large-scale benchmark archive for remote sensing image understanding. In *IEEE International Geoscience and Remote Sensing Symposium (IGARSS)*, pages 5901–5904, 2019. 2, 5, 6
- [46] Xian Sun, Peijin Wang, Wanxuan Lu, Zicong Zhu, Xiaonan Lu, Qibin He, Junxi Li, Xuee Rong, Zhujun Yang, Hao Chang, et al. Ringmo: A remote sensing foundation model with masked image modeling. *IEEE Transactions on Geoscience and Remote Sensing*, 61:1–22, 2023. 3
- [47] Maofeng Tang, Konstantinos Georgiou, Hairong Qi, Cody Champion, and Marc Bosch. Semantic segmentation in aerial imagery using multi-level contrastive learning with local consistency. In *IEEE Winter Conference on Applications of Computer Vision*, pages 3798–3807, 2023. 3
- [48] Yonglong Tian, Dilip Krishnan, and Phillip Isola. Contrastive multiview coding. In *European Conference on Computer Vision (ECCV)*, pages 776–794, 2020. 3
- [49] Zhan Tong, Yibing Song, Jue Wang, and Limin Wang. Videomae: Masked autoencoders are data-efficient learners for self-supervised video pre-training. *Advances in Neural Information Processing Systems (NeurIPS)*, 35:10078–10093, 2022. 3
- [50] Adam Van Etten, Dave Lindenbaum, and Todd M Bacastow. Spacenet: A remote sensing dataset and challenge series. *arXiv preprint arXiv:1807.01232*, 2018. 2, 5, 6, 7
- [51] Stefano Vincenzi, Angelo Porrello, Pietro Buzzega, Marco Cipriano, Pietro Fronte, Roberto Cucu, Carla Ippoliti, Annamaria Conte, and Simone Calderara. The color out of space: learning self-supervised representations for earth observation imagery. In *International Conference on Pattern Recognition (ICPR)*, pages 3034–3041, 2021. 3
- [52] Di Wang, Qiming Zhang, Yufei Xu, Jing Zhang, Bo Du, Dacheng Tao, and Liangpei Zhang. Advancing plain vision transformer toward remote sensing foundation model. *IEEE Transactions on Geoscience and Remote Sensing*, 61:1–15, 2022. 3

- [53] Jue Wang, Yanfei Zhong, and Liangpei Zhang. Change detection based on supervised contrastive learning for high-resolution remote sensing imagery. *IEEE Transactions on Geoscience and Remote Sensing*, 61:1–16, 2023. 3
- [54] Chen Wei, Haoqi Fan, Saining Xie, Chao-Yuan Wu, Alan Yuille, and Christoph Feichtenhofer. Masked feature prediction for self-supervised visual pre-training. In *IEEE Conference on Computer Vision and Pattern Recognition (CVPR)*, pages 14668–14678, 2022. 3
- [55] Zhenda Xie, Zheng Zhang, Yue Cao, Yutong Lin, Jianmin Bao, Zhuliang Yao, Qi Dai, and Han Hu. Simmim: A simple framework for masked image modeling. In *IEEE Conference on Computer Vision and Pattern Recognition (CVPR)*, pages 9653–9663, 2022. 3, 4
- [56] Zhixiang Xue, Xuchu Yu, Anzhu Yu, Bing Liu, Pengqiang Zhang, and Shentong Wu. Self-supervised feature learning for multimodal remote sensing image land cover classification. *IEEE Transactions on Geoscience and Remote Sensing*, 60:1–15, 2022. 3
- [57] Jure Zbontar, Li Jing, Ishan Misra, Yann LeCun, and Stéphane Deny. Barlow twins: Self-supervised learning via redundancy reduction. In *International Conference on Machine Learning (ICML)*, pages 12310–12320, 2021. 3
- [58] Xinyun Zhang, Binwu Zhu, Xufeng Yao, Qi Sun, Ruiyu Li, and Bei Yu. Context-based contrastive learning for scene text recognition. In *AAAI Conference on Artificial Intelligence*, pages 3353–3361, 2022. 3
- [59] Hengshuang Zhao, Yi Zhang, Shu Liu, Jianping Shi, Chen Change Loy, Dahua Lin, and Jiaya Jia. Psanet: Point-wise spatial attention network for scene parsing. In *ECCV*, pages 267–283, 2018. 6